Transmission loss of double panels filled with porogranular materials

Jean-Daniel Chazot[a)]
Centre de Recherche de Royallieu, Université de Technologie de Compiègne, CNRS UMR 6253 Roberval, BP 20529, 60205 Compiègne Cedex, France

Jean-Louis Guyader
Laboratoire Vibrations Acoustique de l'INSA de Lyon, 25 bis, avenue Jean Capelle, 69621 Villeurbanne Cedex, France

(Received 10 April 2009; revised 2 September 2009; accepted 17 September 2009)

Sound transmission through hollow structures found its interest in several industrial domains such as building acoustics, automotive industry, and aeronautics. However, in practice, hollow structures are often filled with porous materials to improve acoustic properties without adding an excessive mass. Recently a lot of interest arises for granular materials of low density that can be an alternative to standard absorbing materials. This paper aims to predict vibro-acoustic behavior of double panels filled with porogranular materials by using the patch-mobility method recently published. Biot's theory is a basic tool for the description of porous material but is quite difficult to use in practice, mostly because of the solid phase characterization. The original simplified Biot's model (fluid-fluid model) for porogranular material permitting a considerable reduction in data necessary for calculation has been recently published. The aim of the present paper is to propose a model to predict sound transmission through a double panel filled with a porogranular material. The method is an extension of a previous paper to take into account the porogranular material through fluid-fluid Biot's model. After a global overview of the method, the case of a double panel filled with expanded polystyrene beads is studied and a comparison with measurements is realized.
 [DOI: 10.1121/1.3245033]

PACS number(s): 43.55.Rg, 43.55.Ev [NX] Pages: 3040–3048

I. INTRODUCTION

Double glazed panels are of great interest to increase sound insulation in several domains. Basically the air gap between the panels permits to decouple the motions of the receiving panel from the excited one. As shown by London in his work on infinite single[1] and double panels,[2] the gain of sound insulation is mainly obtained thanks to the decoupling of the two panels at high frequency. However, at the double panel resonance frequency, the mass-air-mass resonance phenomenon deteriorates the good sound insulation properties of the double panel. On the other hand, Brunskog[3] showed that the effect of the air layer viscosity could have some influence when the air layer thickness is small enough. This phenomenon is, however, not sufficient to improve significantly the sound insulation of a double panel.

Multilayered structures are also widely employed for sound absorption and vibration damping in several applications such as buildings, automobiles, aircraft, etc. These light weight structures are designed to improve sound insulation without adding an excessive mass that is critical in such applications. To predict the vibro-acoustic behavior of these multilayered structures, several methods are available. Analytical formulations have first been used by Guyader and Lesueur[4,5] for orthotropic multilayered plates and by Nilsson and Nilsson[6] for sandwich structures with honeycomb and foam cores. The transfer matrix method described by Munjal and Sastry[7,8] can also be used to predict the response of infinite multilayered poroelastic panels to incident oblique plane waves. However, these methods are not adapted to predict the vibro-acoustic behavior of finite skew plates. On the contrary, the finite element method used by Panneton and Atalla[9] to predict the sound transmission through finite multilayer systems with poroelastic materials is well adapted to model complex finite geometries. Nevertheless, the main drawback of finite element models comes from the significant computational time required. The patch-mobility method (PMM) used by Ouisse *et al.*[10] to couple linear acoustic problems and by Chazot and Guyader[11] to couple vibro-acoustic problems can also be used efficiently. Indeed, the use of a mobility technique permits to characterize each component of the vibro-acoustic problem separately, either analytically or numerically, and then to calculate the global response solving the interaction equation. If one element is modified, only its own characterization has to be calculated before solving interaction equations. In structural coupling, a similar mobility technique has already been used by Moorhouse[12] and by Naji.[13] An extension to energy mobility has also been developed by Orefice *et al.*[14]

In order to improve the sound insulation properties of hollow structures such as double panels, poroelastic materials are also widely employed. The gain in sound insulation obtained by these materials is due to the large viscous and

[a)]Author to whom correspondence should be addressed. Electronic mail: jean-daniel.chazot@utc.fr

thermal dissipations in the pores. In order to model the vibro-acoustic behavior of such materials, homogenized Biot's theory[15] is generally used. This theory enables to take into account the solid and the fluid phase and their elastic, inertial, and visco-thermal interactions. This model have been implemented with the transfer matrix method by Lauriks *et al.*,[16] and with the finite element method by Panneton and Atalla.[17] An enhanced mixed displacement-pressure formulation has also been developed by Atalla *et al.*[18] However, due to the high computation cost still required to implement this model, simplified numerical methods have been developed,[19,20] as well as simplified poroelastic models. Two classical simplifications of Biot's theory can hence be cited: the rigid frame formulation[21] and the limp formulation.[22,23] In both cases, the solid phase elasticity is not taken into account. These two simplifications lead therefore to an equivalent dissipative fluid formulation. However, in the limp formulation, inertial effects of the solid phase are taken into account. Finally, when the solid phase elasticity is taking part in the vibro-acoustic response of the system, it is possible to only neglect the solid phase shear stress. This simplification leads to a fluid-fluid model presented by Chazot and Guyader.[24] This model is well adapted to describe the behavior of materials with a low shear modulus.[25,26]

Recently the interest on granular material has increased and particular granular materials have been studied such as recycled rubber particles.[27] In vibration damping, such materials have proven to be efficient.[28,29] In sound absorption, the behavior of granular materials is similar to poroelastic materials. Classical Biot's theory can thus be employed directly[30] or with the simplified fluid-fluid model[31] for light and non-cohesive porogranular materials.

This paper presents a method to predict the sound transmission through a double panel filled with a porogranular material. It is an extension of the double panel transmission loss (TL) model with the patch-mobility method developed in Ref. 11, when the simplified fluid-fluid model presented in Ref. 24 is used to take into account the porogranular material. After a global overview of the method, the case of a double panel filled with expanded polystyrene beads is studied and a comparison with measurements is realized.

II. VIBRO-ACOUSTIC MODEL OF A DOUBLE PANEL FILLED WITH A POROGRANULAR MATERIAL

In this section, the PMM detailed in Ref. 11 is applied to calculate the vibro-acoustic response of a double panel containing a porogranular material. The double panel is coupled to a cavity and radiates in an open external space (see Fig. 1). Only the main lines of the method are reminded here.

In the PMM, the averaged velocity on patch i of the subsystem A after coupling, $\langle V_A\rangle_i$, is calculated by summing the averaged velocity before coupling $\langle \tilde{V}_A\rangle_i$ and the averaged velocity responses due to coupling surface forces with other subsystems $\langle F_{\tilde{A}/A}\rangle_j$ on patch j such as

$$\langle V_A\rangle_i = \langle \tilde{V}_A\rangle_i + \sum_{j=1}^{N_{AB}} \langle\langle Y_A\rangle\rangle_{ij}\langle F_{\tilde{A}/A}\rangle_j. \tag{1}$$

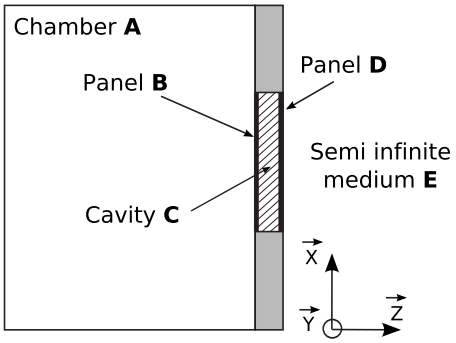

FIG. 1. Sketch of a double panel coupled with a source room and a semi-infinite medium.

The averaged velocity response of the subsystem A on patch i due to a coupling force on patch j is calculated with the patch mobility defined as the ratio of the averaged patch i velocity to the averaged patch j surface force:

$$\langle\langle Y_A\rangle\rangle_{ij} = \frac{\langle V\rangle_i}{\langle F\rangle_j}, \tag{2}$$

where

$$\langle V\rangle_i = \frac{\int_{Si} V(x,y)dxdy}{Si} \tag{3}$$

and

$$\langle F\rangle_j = \frac{\int_{Sj} F(x,y)dxdy}{Sj}. \tag{4}$$

External excitations are taken into account, thanks to the velocities before coupling, and continuity conditions over coupling surfaces are necessary to get rid of the unknown coupling surface forces.

In the case of the double panel containing a porogranular material, the system is first divided into five sub-systems as depicted in Fig. 1: the emission chamber A, the first panel B, the cavity C filled with a porogranular material, the second panel D, and the semi-infinite medium E. Existing coupling surfaces between subsystems i and j are defined: S_{ij}.

The complete set of equations given in Ref. 11 that describes all the physical interactions taking part in the vibro-acoustic response of the double panel can be slightly simplified because the pressure radiated by the panel into the source room is negligible compared to the excitation provided by the source. The coupling of the first panel with the source room is therefore omitted, and the double panel excitation is introduced with a velocity before coupling of the first panel.

For each subsystem, simplified governing equations writes the following.

For the first panel,

$$\langle V_B\rangle_i = \langle \tilde{V}_B\rangle_i + \sum_{j=1}^{N_{BC}} \langle\langle Y_B\rangle\rangle_{ij}\langle F_{C/B}\rangle_j. \tag{5}$$

For the cavity face BC ($\forall i \in S_{BC}$),

$$\langle V_{C1}\rangle_i = \sum_{j=1}^{N_{BC}} \langle\langle Y_{C1}\rangle\rangle_{ij}\langle F_{B/C}\rangle_j + \sum_{k=1}^{N_{CD}} \langle\langle Y_{C1}\rangle\rangle_{ik}\langle F_{D/C}\rangle_k. \quad (6)$$

For the cavity face CD ($\forall i \in S_{CD}$),

$$\langle V_{C2}\rangle_i = \sum_{k=1}^{N_{CD}} \langle\langle Y_{C2}\rangle\rangle_{ik}\langle F_{D/C}\rangle_k + \sum_{j=1}^{N_{BC}} \langle\langle Y_{C2}\rangle\rangle_{ij}\langle F_{B/C}\rangle_j. \quad (7)$$

For the second panel,

$$\langle V_D\rangle_i = \sum_{k=1}^{N_{CD}} \langle\langle Y_D\rangle\rangle_{ik}\langle F_{C/D}\rangle_k. \quad (8)$$

Excitation appears in Eq. (5) as a patch velocity vector before coupling $\langle \tilde{V}_B\rangle_i$. It is calculated from plate B patch transfer mobility (PTM) $\langle\langle Y_B\rangle\rangle_{ij}$, and from boundary pressure in the source room, as

$$\langle \tilde{V}_B\rangle_i = \sum_j \langle\langle Y_B\rangle\rangle_{ij}\langle P_{(\text{blocked})}\rangle_j S_j, \quad (9)$$

where blocked patch pressures $\langle P_{(\text{blocked})}\rangle_j$ are calculated by integrating over patches the pressure, generated by a source in the emission chamber, over the panel assumed to be rigid (blocked).

Finally, velocity continuity conditions over coupling surfaces S_{BC} and S_{CD} are written: $\forall i \in S_{BC}$: $\langle V_B\rangle_i = \langle V_C\rangle_i$ and $\forall i \in S_{CD}$: $\langle V_C\rangle_i = \langle V_D\rangle_i$. It yields to

$$\begin{Bmatrix} \langle \tilde{V}_1\rangle_i \\ 0 \end{Bmatrix} = [\mathbf{Y}] \begin{Bmatrix} \langle F_{B/C}\rangle_j \\ \langle F_{D/C}\rangle_k \end{Bmatrix} \quad (10)$$

with

$$[\mathbf{Y}] = \begin{bmatrix} \langle\langle Y_{C1}\rangle\rangle_{ij} + \langle\langle Y_B\rangle_i\rangle_j & \langle\langle Y_{C1}\rangle\rangle_{ik} \\ \langle\langle Y_{C2}\rangle\rangle_{ij} & \langle\langle Y_{C2}\rangle\rangle_{ik} + \langle\langle Y_D\rangle\rangle_{ik} \end{bmatrix}.$$

Solving the linear system (10) allows to get coupling forces $\langle F_{B/C}\rangle_j$ and $\langle F_{D/C}\rangle_k$ and then to calculate patch velocities after coupling by using Eqs. (5)–(8).

Sections III–V present the panel patch mobilities, porogranular patch mobilities, and radiation patch mobilities that are used to calculate the response of the double panel filled with a porogranular material. In all the following calculations, harmonic motions of angular frequency ω are assumed, and for sake of simplicity, time dependence $e^{+j\omega t}$ is omitted.

III. PANEL PATCH MOBILITIES

The panel patch mobility can be calculated from the Love–Kirchhoff equation of motion (flexural vibration of thin plates) using a modal expansion of the plate transverse displacement with simply supported boundary conditions. Details of these calculations are given in Ref. 11. The panel patch mobility hence obtained writes

$$\langle\langle YP\rangle\rangle_{ij} = \frac{j\omega}{S_i S_j}\sum_{pq} \frac{\int_{S_i}\Phi_{pq}(x,y)dS \cdot \int_{S_j}\Phi_{pq}(x,y)dS}{M_{pq}[\omega_{pq}^{*2} - \omega^2]}, \quad (11)$$

where

$$K_{pq}^* = \int_S D^*\Phi_{pq}\nabla^4(\Phi_{pq})dS, \quad M_{pq} = \int_S \rho h \Phi_{pq}^2 dS,$$

$$\omega_{pq}^* = \sqrt{\frac{K_{pq}^*}{M_{pq}}}, \quad D^* = \frac{E^* h^3}{12(1-\nu^2)}.$$

E^* is complex Young modulus which takes into account structural damping such as $E^* = E(1+j\eta_s)$, and η_s is the damping loss factor. Mode shapes of simply supported plates are used: $\Phi_{pq}(x,y) = \sin((p\pi/L_x)x)\sin((q\pi/L_y)y)$, where L_x and L_y are the plate dimensions. In some cases, and, in particular, for a diffuse field excitation with large panel dimensions, the transmission loss of the panel does not depend on the boundary conditions. However, as mentioned in Refs. 32 and 33, real boundary conditions have to be taken into account at low frequency and for small panel dimensions. A modal expansion of clamped panel given in Ref. 32 can then be used.

IV. POROGRANULAR PATCH MOBILITIES

Different simplifications can be brought to full Biot's theory depending on the studied material elastic characteristics. A simplification was hence proposed in Ref. 24 to model light and non-cohesive porogranular materials. The basic idea of this model is to modify the elastic law of the solid phase to suppress shear stresses. The granular material phase is also assumed to behave like a fluid with a hydrostatic stress tensor such as $\sigma^s = -p_s I$, with I the identity matrix and p_s the equivalent solid pressure that represents the hydrostatic stress of the granular material phase. The resulting fluid-fluid model is presented in Eq. (12).

$$\begin{aligned} &[A\Delta p_s + p_s] + B\Delta p = 0 \\ &[C\Delta p + p] + D\Delta p_s = 0 \end{aligned} \quad \text{on } \Omega$$

$$\mathbf{V_s}\cdot\mathbf{n} = \mathbf{V_f}\cdot\mathbf{n} = \begin{cases} \langle V_n\rangle_j & \text{on excitation patch } j \\ 0 & \text{elsewhere} \end{cases} \quad \text{on } \partial\Omega \quad (12)$$

p_s and $\mathbf{V_s}$ stand for the equivalent pressure and velocity in the solid phase, p and $\mathbf{V_f}$ are the fluid pressure and velocity, $\mathbf{n}$ denotes here the outward normal unit vector to the poroelastic domain, and A, B, C, and D are elastic coefficients given in Appendix B. These coefficients are related to elastic and inertial coupling coefficients.

Boundary conditions given on the surface $\partial\Omega$ are chosen to obtain the transfer impedance between two patches i and j. A uniform normal velocity $\langle V_n\rangle_j$ is therefore applied on excitation patch j, and the resulting pressure p_t is averaged over observation patch i. These boundary conditions are then applied over the porogranular material using coupling conditions by considering an elastic-poroelastic interface as defined in Ref. 34. The resulting coupling conditions are given

by Eq. (13). These equations are based on the flow, the fluid velocity, and the total normal stress continuity conditions. On excitation patch, the solid and fluid normal velocities are thus equal to the normal excitation velocity, while the total pressure over the observation patch is given by the average pressure over the two phases.

$$\mathbf{V_s}\cdot\mathbf{n}\begin{cases}\langle V_n\rangle_j & \text{on excitation patch } j\\ 0 & \text{elsewhere,}\end{cases}$$

$$\mathbf{V_f}\cdot\mathbf{n}\begin{cases}\langle V_n\rangle_j & \text{on excitation patch } j\\ 0 & \text{elsewhere,}\end{cases} \tag{13}$$

$$\langle p_t\rangle_i = (1-\phi)\langle p_s\rangle_i + \phi\langle p\rangle_i,$$

where ϕ is the porosity and the normal averaged velocity $\langle V_n\rangle_j$ is considered constant on patch j. The solid and fluid velocities, $\mathbf{V_s}$ and $\mathbf{V_f}$, used in boundary conditions are also related to the solid and fluid pressure gradients through Eq. (14):

$$\begin{aligned}(1-\phi)\nabla p_s &= -(\rho_{11}\mathbf{V_s}+\rho_{12}\mathbf{V_f})j\omega,\\ \phi\nabla p &= -(\rho_{12}\mathbf{V_s}+\rho_{22}\mathbf{V_f})j\omega.\end{aligned} \tag{14}$$

In order to obtain the weak formulation associated with the fluid-fluid model, Eq. (12) are multiplied with a trial function and integrated over the domain Ω. Green's identities enable then to introduce the boundary conditions leading to the weak formulation given in Eq. (15):

$$\begin{aligned}&\int_\Omega (A\Delta\Psi_s+\Psi_s)p_s d\Omega - \int_{\partial\Omega} A(\nabla\Psi_s p_s)\mathbf{n}dS\\ &\quad - j\omega A\frac{\rho_{11}+\rho_{12}}{1-\phi}\langle\Psi_s\rangle_j\langle V_n\rangle_j S_j + \int_\Omega B(p\Delta\Psi_s)d\Omega\\ &\quad - \int_{\partial\Omega} B(\nabla\Psi_s p)\mathbf{n}dS - j\omega B\frac{\rho_{12}+\rho_{22}}{\phi}\langle\Psi_s\rangle_j\langle V_n\rangle_j S_j = 0,\\ &\int_\Omega (C\Delta\Psi+\Psi)p d\Omega - \int_{\partial\Omega} C(\nabla\Psi p)\mathbf{n}dS\\ &\quad - j\omega C\frac{\rho_{12}+\rho_{22}}{\phi}\langle\Psi\rangle_j\langle V_n\rangle_j S_j + \int_\Omega D(p_s\Delta\Psi)d\Omega\\ &\quad - \int_{\partial\Omega} D(\nabla\Psi p_s)\mathbf{n}dS - j\omega D\frac{\rho_{11}+\rho_{12}}{1-\phi}\langle\Psi\rangle_j\langle V_n\rangle_j S_j = 0,\end{aligned} \tag{15}$$

where Ψ_s and Ψ are the solid and fluid test functions. Averaged test functions write $\langle\Psi_s\rangle_j=\int_{s_j}\Psi_s dS/S_j$ and $\langle\Psi\rangle_j=\int_{s_j}\Psi dS/S_j$.

The Rayleigh–Ritz method is then applied to the weak formulation of fluid-fluid Biot's model, and modal expansions of the solid and fluid pressure fields are introduced:

$$p_s(M) = \sum_{pqr} a_{pqr}\cdot\psi_{pqr}(M), \tag{16}$$

$$p(M) = \sum_{pqr} b_{pqr}\cdot\psi_{pqr}(M). \tag{17}$$

The fluid pressure is hence decomposed over the basis of rigid-walled cavity mode shapes $\psi_{pqr}(M)$ such as $\psi_{pqr}(M)=\cos(p\pi x/L_x)\cos(g\pi y/L_y)\cos(r\pi z/L_z)$, with L_x, L_y, and L_z the cavity dimensions. The solid phase being also assumed to behave like a fluid, the equivalent solid pressure p_s is decomposed over the same basis. Notice also that velocity boundary conditions can be employed in the weak formulation (15) with a basis of rigid-walled cavity mode shapes. The resulting velocity field will then be incorrect locally on the excitation patch, but the weak formulation ensures, however, that the pressure response is correct. Thus, it is possible to calculate the impedance matrix [Eq. (21)] and finally to obtain the mobility matrix by inversion [Eq. (22)].

Solid and fluid test functions are also replaced by a mode shape $\psi_{pqr}(M)$:

$$\begin{aligned}\Psi_s &= \psi_{pqr}(M),\\ \Psi &= \psi_{pqr}(M).\end{aligned} \tag{18}$$

Modal orthogonality and null normal derivatives of test functions on the boundary surfaces lead the Rayleigh–Ritz method associated with the weak formulation (15) to Eq. (19).

$$\begin{aligned}a_{pqr} &= \frac{Bk_{pqr}^2 N_{pqr}}{I_{pqr}}b_{pqr} + \left(\frac{A}{I_{pqr}}\cdot\frac{\rho_{11}+\rho_{12}}{1-\phi} + \frac{B}{I_{pqr}}\cdot\frac{\rho_{22}+\rho_{12}}{\phi}\right)\\ &\quad\times j\omega\langle V_n\rangle_j\langle\psi_{pqr}\rangle_j S_j,\\ b_{pqr} &= \left(\frac{D}{J_{pqr}}\cdot\frac{\rho_{11}+\rho_{12}}{1-\phi} + \frac{(BD-AC)k_{pqr}^2+C}{J_{pqr}}\cdot\frac{\rho_{22}+\rho_{12}}{\phi}\right)\\ &\quad\times j\omega\langle V_n\rangle_j\langle\psi_{pqr}\rangle_j S_j,\end{aligned} \tag{19}$$

with $k_{pqr}^2=(p\pi/L_x)^2+(q\pi/L_y)^2+(r\pi/L_z)^2$, $I_{pqr}=N_{pqr}(1-Ak_{pqr}^2)$, $J_{pqr}=N_{pqr}(1-(A+C)k_{pqr}^2+(AC-BD)k_{pqr}^4)$, and $N_{pqr}=\int_\Omega\psi_{pqr}^2 d\Omega$.

The total averaged pressure on patch i is therefore given by

$$\langle p_t\rangle_i = \sum_{pqr}((1-\phi)a_{pqr}+\phi b_{pqr})\langle\psi_{pqr}\rangle_i, \tag{20}$$

and Patch transfer impedance writes

$$\langle\langle Z\rangle\rangle_{ij} = \frac{\langle p_t\rangle_i S_i}{\langle V_n\rangle_j}. \tag{21}$$

Porogranular patch mobilities can finally be deduced by inverting the patch transfer impedance matrix:

$$[Y] = [Z]^{-1}. \tag{22}$$

V. RADIATED POWER INTO THE SEMI-INFINITE MEDIUM

Radiated power is calculated from patch velocities and radiated patch pressures, and can be written using radiation patch impedances (23):

$$\Pi_{\text{rad}} = \frac{1}{2}\sum_i \text{Re}\{\langle V\rangle_i^*\langle P_{\text{rad}}\rangle_i S_i\},$$

$$= \frac{1}{2}(\mathrm{Re}[Z_{\mathrm{rad}}])\{V\}'\{V_i S_i\}^*. \quad (23)$$

The expressions of the radiation patch impedances are given in Appendix A.

VI. TRANSMISSION LOSS CALCULATIONS

A standard room response modal expansion is used to calculate the mean quadratic room pressure P_r^2 and the blocked patch pressures $\langle P\rangle_i$ over the incident panel. The resulting expressions are, respectively, given in Eqs. (24) and (25). Mode shapes ψ_{pqr} of a parallelepipedic-shaped room with rigid walls are used, and detailed calculations of modal amplitudes A_{pqr} are given in Ref. 11.

$$P_r^2 = \sum_{pqr} \frac{|A_{pqr}^2|\varepsilon_p\varepsilon_q\varepsilon_r}{8}, \quad (24)$$

with

$$\varepsilon_p = \begin{cases} 1 & \text{if } p = 0 \\ 2 & \text{if } p \neq 0, \end{cases}$$

$$\langle P\rangle_i = \int_{Si} \left(\sum_{p,q,r} A_{pqr}\psi_{pqr}(x,y,z) \right) dS. \quad (25)$$

The blocked patch pressures are used in Eq. (9) to calculate panel patch velocities before coupling, and enable to solve the set of Eqs. (5)–(8). As stated in Ref. 11, the great advantage of using blocked patch pressures instead of summing incident plane waves is to avoid the integration of plane waves over incidence angles to model a diffuse field leading to tremendous calculation time compared to the present method. Moreover, the blocked patch pressure calculation depends only on the source room configuration and is totally separated from the transmission loss calculations of a panel. Hence, once the source room is characterized with blocked patch pressures, transmission loss calculation of any panel is possible.

Finally, using the mean quadratic room pressure and radiated patch pressures, the panel transmission loss can be calculated. TL is indeed defined as the ratio of transmitted power Π_t to incident power Π_i: $\mathrm{TL} = 10\log(\Pi_i/\Pi_t)$. Transmitted power can be calculated, thanks to the mobility method with Eq. (23). On the other hand, according to the procedure of standard measurement of transmission loss, incident power is deduced from mean quadratic room pressure using a classical result of Sabine's theory: $\Pi_i = SP_r^2/4\rho_0 c$. Of course the assumption of Sabine's theory is not exactly verified for standard rectangular rooms especially at low frequency, but is nevertheless of general use for sake of simplicity.

VII. RESULTS

A. Calculated porogranular patch mobilities

The porogranular material we used was made of expanded polystyrene beads non-cohesive and of low density (19 kg/m^3). Its properties are given in Table I. These data come from Ref. 24 where the measurement technique is also reported. It is based on impedance tube measurements when no preload is applied to the granular material. When the material is maintained in a limited space with an initial load due to the gravity or to the experimental mounting, the bulk modulus can increase like in a fluid submitted to a pressure load. The chosen value of the bulk modulus is discussed in Sec. VII B.

TABLE I. Parameters of the porogranular material (after Ref. 24).

Parameter	Value
Porosity ϕ	0.41
Tortuosity α_∞	1.2855
Permeability k_0	9.29×10^{-9} m^2
Viscous characteristics length Λ	0.2 mm
Thermal characteristic length Λ'	0.34 mm
Bulk modulus	$0.35(1+0.18i)$ MPa.

The comparison of patch input mobilities of porogranular material and air cavity is presented in Fig. 2. The magnitude of the patch input mobility of the porogranular material appears to be lower than the air cavity. This is due to higher stiffness of the porogranular material. On the other hand, the phase of the air cavity input mobility is constant around 90 while the phase of the porogranular input mobility decreases with frequency. This phase illustrates the total dissipations, viscous and thermal, that take place in the porogranular material. Indeed, the media does not dissipate energy when the phase is equal to 90, and dissipations appear when the phase is different from 90. The porogranular material is therefore more dissipative at high frequency than at low frequency.

Surprisingly also, patch mobilities do not exhibit a modal behavior in the studied frequency band. In Ref. 24, this non-modal behavior is explained by the fact that direct patch-mobility calculation derives from a Dirichlet problem with a null boundary pressure except on excited patch. Cavity resonances with Dirichlet boundary conditions are obviously different from that of a cavity with Neumann boundary conditions. The first resonance of the rectangular cavity with Dirichlet boundary conditions is equal to $c/2\pi \times\sqrt{(pi/L_x)^2+(pi/L_y)^2+(pi/L_z)^2}$ that is to say 17 000 Hz. That explains why no resonance appears in the studied frequency band, even if our calculation is indirect and use inverse impedance matrix calculated with rigid wall cavity basis.

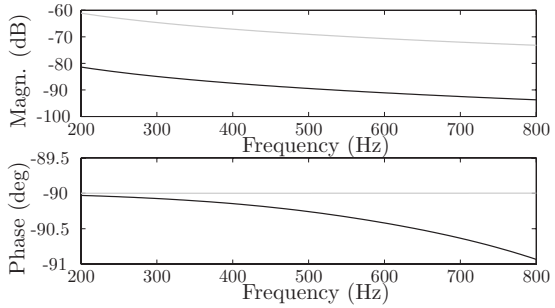

FIG. 2. Patch input mobility—black line: porogranular mobility; gray line: air cavity mobility (after Ref. 11)—patch 42—cavity: L_x=1.5 m, L_y=0.96 m, L_z=0.01 m—patch size: Δx=7.9 cm, Δy=7.4 cm—Patch 42: X=[0.24 m;0.32 m], Y=[0.15 m;0.22 m].

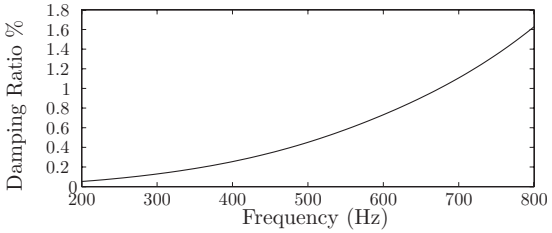

FIG. 3. Damping ratio evaluated from the patch input mobility—patch 42—cavity: L_x=1.5 m, L_y=0.96 m, L_z=0.01 m—patch size: Δx=7.9 cm, Δy=7.4 cm—patch 42: X=[0.24 m;0.32 m], Y=[0.15 m;0.22 m].

To quantify the damping associated with the porogranular material, the patch input impedance is identified as a complex stiffness K^* with an imaginary part characterized by a damping loss factor η such as $K^*=K(1+j\eta)$. The corresponding mobility has the following form:

$$Y = -\frac{j\omega S}{K(1+j\eta)}. \tag{26}$$

One can deduce that $\eta=\mathrm{Re}(Y)/\mathrm{Im}(Y)$. This damping loss factor η presented in Fig. 3 shows the expected ability of the porogranular material to dissipate energy. The damping loss factor is increasing with frequency and reach 0.016 at 800 Hz. Of course this analysis only characterizes the dissipation observed at a given patch, and cannot be seen as a complete characterization of the damping properties of the porogranular material that is not under study in this paper. However, the dissipation is of major importance to limit the transmission at the mass-air mass frequency.

In Fig. 4, the patch transfer mobility (PTM) of a porogranular material and air cavity are compared. The magnitude of the PTM is lower for the porogranular material due to a higher stiffness. However, the phase of the porogranular transfer mobility varies with frequency. These variations are related to the propagation time of solid and fluid waves between excitation and observation points and also to viscothermal dissipations inside the material.

B. Comparison of measured and calculated TL

Figure 5 presents the experimental setup. Measurements of transmitted power were done using intensity technique with a 50 mm intensity probe located at 20 cm from the

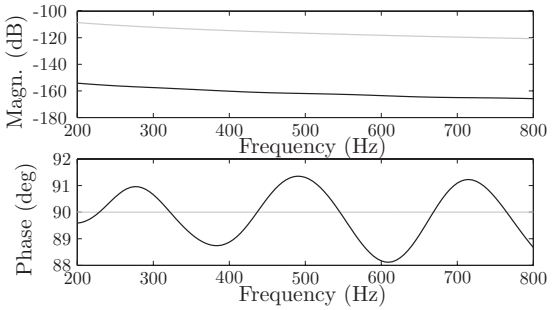

FIG. 4. Patch transfer mobility—black line: porogranular mobility; gray line: air cavity mobility (after Ref. 11)—patches 42 and 72—cavity: L_x=1.5 m, L_y=0.96 m, L_z=0.01 m—patch size: Δx=7.9 cm, Δy=7.4 cm—patch 42: X=[0.24 m;0.32 m], Y=[0.15 m;0.22 m], Z=0—patch 72: X=[1.11 m;1.18 m], Y=[0.22 m;0.30 m], Z=0.01 m.

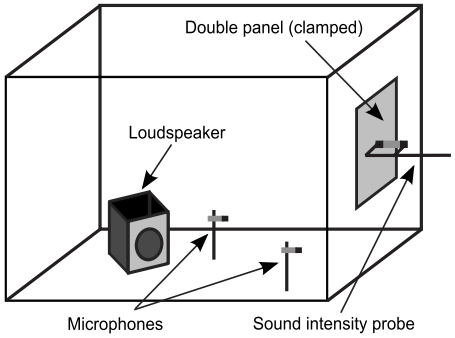

FIG. 5. Experimental setup.

radiating panel. 100 points have been used to measure radiated intensity. Source room is a large reverberant room (lx=11.5 m, ly=8.69 m, lz=4.03 m, cutt off frequency =187 Hz) where walls are not parallel and with diffusers in the corners. Five microphones in the reverberant chamber enabled to measure reverberant pressure. Receiving room is a large anechoic space treated to be isolated from exterior noise.

Transmission loss of a double aluminum panel filled with a porogranular material was measured. The double panel dimensions were as follows: width 0.96 m, length 1.5 m, thicknesses 2 and 1.5 mm, intermediate cavity thickness 1 cm. Panel critical frequencies are 7961 Hz (respectively, 5971 Hz) for the aluminum panel of 1.5 mm (respectively, 2 mm) thickness. The porogranular material tested was made of expanded polystyren beads of very low density (19 kg/m^3) and non-cohesive. Acoustic parameters of this material are given in Table I.

The experiment presents the case of a cavity not fully filled in order to allow a relative motion between beads. It is indeed important to not couple the two panels in order to keep the good insulation properties of the double panel. A small gap of air is hence kept at the top of the cavity. However, due to gravity a small preload on the porogranular material exists.

Figure 6 presents comparative transmission loss of a double panel measured and calculated with the patch-mobility method. The model gives good comparative results. The bulk modulus of the porogranular material solid phase given in Ref. 24 has, however, been modified to get these results. As mentioned previously, the material being maintained in a limited space with an initial load, the bulk modulus is also increased compared to data in Ref. 24, obtained in standing wave tube, on a layer of porogranular material totally free of compression. A good comparison of transmission loss was observed for a bulk modulus increased to 0.35 MPa.

Moreover, the bulk modulus depends also on the behavior of the granular material. Basically, three behaviors can be distinguished:[35] quasistatic, rapid granular flow, and intermediate behaviors. In the present case of a cavity not fully filled with a light porogranular material, the intermediate behavior is the more likely. Indeed, the beads can slightly move in the cavity but a rapid granular flow is not possible due to the small cavity thickness and to the small acoustic displace-

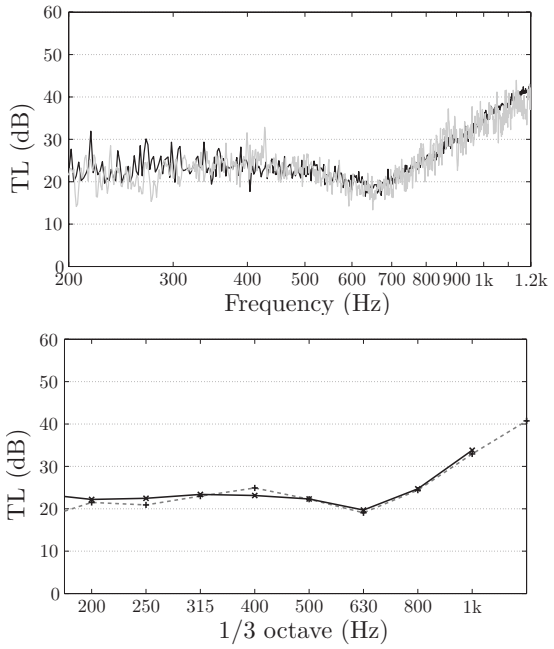

FIG. 6. Comparison with experiment—black line: model; gray line: experiment—double aluminum panel (L_x=0.96 m, L_z=1.5 m), 2 and 1.5 mm thickness, separated by a cavity of 1 cm filled with expanded polystyrene beads, centered on point X=6 m, Y=0 m, Z=1.75 m—room dimensions: lx=11.5 m, ly=8.69 m, lz=4.03 m—patch size: ΔX=0.08 m, ΔZ=0.074 m—source at Xs=2 m, Ys=4 m, Zs=1 m, amplitude: S_0=2—cut off frequency: 187 Hz—structural damping: 0.01.

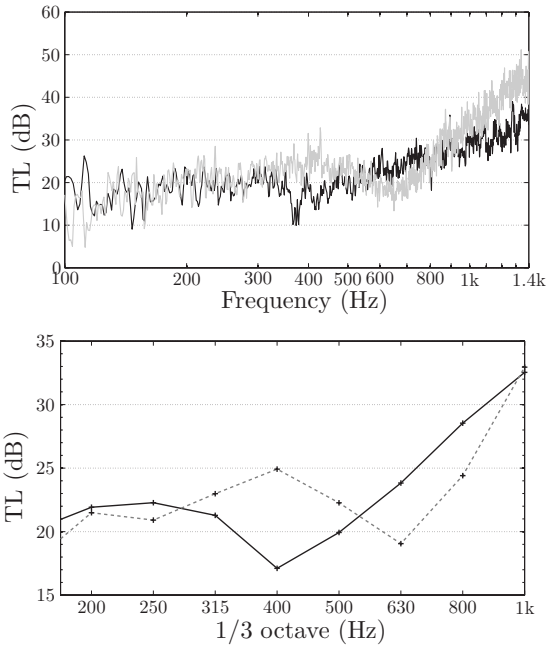

FIG. 7. Experimental comparisons—black solid line: air cavity; gray dotted line: cavity filled with expanded polystyrene beads—double aluminum panel (L_x=0.96 m, L_z=1.5 m), 2 and 1.5 mm thickness, separated by a cavity of 1 cm, centered on point X=6 m, Y=0 m, Z=1.75 m—room dimensions: lx=11.5 m, ly=8.69 m, lz=4.03 m—source at Xs=2 m, Ys=4 m, Zs=1 m—cut off frequency: 187 Hz.

ments. However, if the filling of the cavity is increased, the preload on the material can increase due to a compacting of the beads and the quasistatic behavior can become predominant. In that case, it will be necessary to change the bulk modulus in the model in order to take into account this change of behavior. However, a linear increase in the bulk modulus with the preload is unlikely because of the point contact between the beads. This non-linear behavior is, for example, well known for fibrous materials where the apparent stiffness depends on the strain level at which the sample is tested.[36]

Figure 7 presents a comparison of experimental results obtained for double panels filled with a porogranular material and with an air cavity. In the case of a cavity filled with a porogranular material, the dip at mass-air-mass resonance frequency is visible at 630 Hz instead of 400 Hz. This slight increase is due to the stiffness added by the porogranular material. At higher frequency, the increase of TL is still present and confirms that higher stiffness does not suppress the double plate behavior. Moreover, the transmission loss gradient after the mass-air-mass resonance frequency is increased of 40% with the porogranular material. This study on a standard granular material shows therefore that the TL of a double panel can be improved. However, this particular case is certainly not the optimal combination of material and cavity filling. Indeed, the frequency resonance can still be modified and adapted through the material properties and the cavity filling. Practical applications in building and transportation industries of hollow panels filled with porogranular material are therefore promising.

VIII. CONCLUSIONS

In this paper, the patch-mobility method was used to predict the sound transmission loss through finite double panels filled with a porogranular material. Porogranular material was taken into account with Biot's fluid-fluid model based on a simplification of the standard Biot's poroelastic model. This simplification was an alternative to other simplifications like the limp model or the rigid frame model. It permitted to neglect the shear stress and to take into account the solid frame stiffness in order to describe the double panel behavior. Numerical results obtained with this model were compared to transmission loss measurements made on a double aluminum panel including expanded polystyrene beads. It appeared hence that the TL trends were correctly predicted by this model. However, a modified bulk modulus was necessary to take into account the static compression of beads induced by the mounting of the double panel. Finally, very light porogranular materials placed in double plate cavity appeared to be an interesting way to improve sound insulation through double panels.

APPENDIX A: RADIATION PATCH IMPEDANCE

The radiation patch impedance $\langle\langle Z\rangle\rangle_{ij}$ is defined as the ratio of averaged patch i radiated pressure to averaged patch j velocity: $\langle\langle Z\rangle\rangle_{ij}=\langle P_{\mathrm{rad}}\rangle_i/\langle V\rangle_j$.

Calculations are based on Rayleigh's integral and are detailed in Ref. 11. When emitting and receiving patches are different (i.e., $i\neq j$), Eq. (A1) is used to calculate radiation impedance where d_{ij} is the distance between two patches central points. A particular case is defined when emitting and receiving patches are the same (i.e., $i=j$). In this case, radia-

tion impedance expression is given by Eq. (A2) where a_i is the radius of a circular patch of surface S_i. The approximation employed to get these expressions is valid for small enough patch surface, and in general a discretization based on the standard $\lambda/6$ criterion is sufficient.

$$\langle\langle Z\rangle\rangle_{ij} = \frac{\langle P_{\text{rad}}\rangle_i}{\langle V\rangle_j} = \frac{1}{2\pi}\rho_0 j \frac{\exp^{-jkd_{ij}}}{d_{ij}} S_j, \tag{A1}$$

$$\langle\langle Z\rangle\rangle_{ii} = \frac{\langle P_{\text{rad}}\rangle_i}{\langle V\rangle_i} = \rho_0 c[1 - \exp^{-jka_i}]. \tag{A2}$$

APPENDIX B: FLUID-FLUID MODEL

The presented fluid-fluid model is detailed in Ref. 24. Elastic coefficients used in the fluid-fluid model write

$$A = F(P\rho_{22} - Q\rho_{12}), \quad B = F(-P\rho_{12} + Q\rho_{11})\phi/(1-\phi),$$

$$C = F(-Q\rho_{12} + R\rho_{11}), \quad D = F(Q\rho_{22} - R\rho_{12})(1-\phi)/\phi, \tag{B1}$$

$$F = [(\rho_{22}\rho_{11} - \rho_{12}^2)\omega^2]^{-1}.$$

These coefficients are related to the porosity ϕ, elastic coefficients P, Q, and R, and equivalent densities ρ_{ij}. Elastic coefficients and equivalent densities are standard coefficients used in Biot–Allard's formulation with time dependence $e^{+j\omega t}$ and are, respectively, recalled in Eqs. (B2) and (B3).

$$P = \frac{4}{3}N + K_b + \frac{(1-\phi)^2}{\phi}K_f,$$

$$Q = \frac{R(1-\phi)}{\phi}, \tag{B2}$$

$$R = \phi K_f,$$

$$\rho_{11} = \rho_s + \phi(\rho_f - \rho_0),$$

$$\rho_{12} = \phi(\rho_0 - \rho_f), \tag{B3}$$

$$\rho_{22} = \phi\rho_f.$$

N, K_b, and ρ_s are, respectively, the shear modulus, the bulk modulus, and the density of the solid frame. Viscous and thermal dissipations are, respectively, taken into account by frequency dependent expressions of fluid density ρ_f and dynamic fluid compressibility K_f. Johnson–Allard's expressions[37] given in Eq. (B4) are used to describe the microgeometry structure with five parameters: porosity ϕ, tortuosity α_∞, viscous permeability k_0 (related to air flow resistivity by $\sigma = \eta/k_0$ with k_0 the dynamic fluid viscosity), and viscous and thermal characteristic lengths (respectively, Λ and Λ'). Pr is the Prandtl number.

$$\rho_f = \rho_0\alpha_\infty\left(1 + \frac{\eta\phi}{j\rho_0\alpha_\infty k_0\omega}\sqrt{1 + 4\frac{k_0^2\alpha_\infty^2 j\omega\rho_0}{\Lambda^2\phi^2\eta}}\right), \tag{B4}$$

$$K_f = \frac{\gamma P_0}{\gamma - (\gamma-1)\left(1 + \frac{8\eta}{j\Lambda'^2\,\text{Pr}\,\omega\rho_0}\sqrt{1 + j\rho_0\frac{\text{Pr}\,\Lambda'^2\omega}{16\eta}}\right)^{-1}}.$$

However, two different definitions can be employed for the elastic coefficient P. If one considers a light and noncohesive porogranular material without shear stress, the elastic coefficient P stands for the skeleton bulk modulus with a coupling part due to the fluid phase: $P = K_b + ((1-\phi)^2/\phi)K_f$. Compared to the classical coefficient P used in Biot's model, the shear term $\frac{4}{3}N$ has been removed by simply considering a fluid behavior in the stress-strain relations (i.e., hydrostatic stress tensor). On the contrary, when the aim is to neglect the shear stress in a material that does not behave like a fluid, it is also possible to keep the same coefficient P than the one used in Biot's formulation: $P = (4/3)N + K_b + ((1-\phi)^2/\phi)K_f$. This enables to keep the same dispersion equation in both formulations. Of course, when N is very small compared to $K_b + ((1-\phi)^2/\phi)K_f$, both definitions of P are similar. In the following, the first definition is employed.

[1] A. London, "Transmission of reverberant sound through single walls," J. Res. Natl. Bur. Stand. **42**, 605–615 (1949).
[2] A. London, "Transmission of reverberant sound through double walls," J. Acoust. Soc. Am. **22**, 270–279 (1950).
[3] J. Brunskog, "The influence of finite cavities on the sound insulation of double-plate structures," J. Acoust. Soc. Am. **117**, 3727–3739 (2005).
[4] J. Guyader and C. Lesueur, "Acoustic transmission through orthotropic multilayered plates, part ii: Transmission loss," J. Sound Vib. **58**, 69–86 (1978).
[5] J. Guyader and C. Lesueur, "Transmission of reverberant sound through orthotropic viscoelastic multilayered plates," J. Sound Vib. **70**, 319–332 (1980).
[6] E. Nilsson and A. Nilsson, "Prediction and measurement of some dynamic properties of sandwich structures with honeycomb and foam cores," J. Sound Vib. **251**, 409–430 (2002).
[7] M. Munjal, "Response of a multi-layered infinite plate to an incident oblique plane wave by means of transfer matrices," J. Sound Vib. **162**, 333–343 (1993).
[8] J. Sastry and M. Munjal, "A transfer matrix approach for evaluation of the response of a multi-layer infinite plate to a two-dimensional pressure excitation," J. Sound Vib. **182**, 109–128 (1995).
[9] R. Panneton and N. Atalla, "Numerical prediction of sound transmission through finite multilayer systems with poroelastic materials," J. Acoust. Soc. Am. **100**, 346–354 (1996).
[10] M. Ouisse, L. Maxit, C. Cacciolati, and J. Guyader, "Patch transfer functions as a tool to couple linear acoustics problems," ASME J. Vibr. Acoust. **127**, 458–466 (2005).
[11] J. Chazot and J. Guyader, "Prediction of transmission loss of double panels with a patch-mobility method," J. Acoust. Soc. Am. **121**, 267–278 (2007).
[12] A. T. Moorhouse, "A dimensionless mobility formulation for evaluation of force and moment excitation of structures," J. Acoust. Soc. Am. **112**, 972–980 (2002).
[13] S. Naji, "Etude des transmissions vibratoires par une méthode de mobilité mixte dans les assemblages par surface (Study on vibration transmissions with a mobility method)," Ph.D. thesis, Universit Claude Bernard Lyon I (1993).
[14] G. Orefice, C. Cacciolati, and J. Guyader, "The energy mobility," J. Sound Vib. **254**, 269–295 (2002).
[15] M. Biot, "Generalized theory of acoustic propagation in porous dissipative media," J. Acoust. Soc. Am. **34**, 168–178 (1962).
[16] W. Lauriks, A. Cops, J. Allard, C. Depollier, and P. Rebillard, "Modelization at oblique incidence of layered porous materials with impervious screens," J. Acoust. Soc. Am. **87**, 1200–1206 (1990).
[17] R. Panneton and N. Atalla, "An efficient finite element scheme for solving the three dimensional poroelasticity problem in acoustics," J. Acoust. Soc. Am. **101**, 3287–3298 (1997).
[18] N. Atalla, R. Panneton, and P. Debergue, "A mixed displacement-pressure

formulation for poroelastic materials," J. Acoust. Soc. Am. **104**, 1444–1452 (1998).
[19]L. Jaouen, B. Brouard, N. Atalla, and C. Langlois, "A simplified numerical model for a plate backed by a thin foam layer in the low frequency range," J. Acoust. Soc. Am. **280**, 681–698 (2005).
[20]O. Dazel, C. Sgard, F. Lamarque, and N. Atalla, "An extension of complex modes for the resolution of finite-element poroelastic problems," J. Sound Vib. **253**, 421–445 (2002).
[21]C. Zwikker and C. Kosten, *Sound Absorbing Materials* (Elsevier, New York, 1949).
[22]L. Beranek, "Acoustical properties of homogeneous isotropic rigid tiles and flexible blankets," J. Acoust. Soc. Am. **19**, 556–568 (1947).
[23]O. Doutres, N. Dauchez, J. Gnevaux, and O. Dazel, "Validity of the limp model for porous materials: A criterion based on the Biot theory," J. Acoust. Soc. Am. **122**, 2038–2048 (2007).
[24]J. Chazot and J. Guyader, "Acoustic modeling of light and non-cohesive poro-granular materials with a fluid/fluid model," Acta Mech. **195**, 227–247 (2008).
[25]B. Nennig, J. Chazot, E. Perrey-Debain, and M. Ben Tahar, "Influence of solid phase elasticity in poroelastic liners submitted to grazing flows," in Proceedings of Euronoise, Paris, France (2008).
[26]B. Nennig, J. Chazot, E. Perrey-Debain, and M. Ben Tahar, "Evaluation of simplified poroelastic models," in Proceedings of SAPEM, Bradford, UK (2008).
[27]Z. Hong, L. Bo, H. Guangsu, and H. Jia, "A novel composite sound absorber with recycled rubber particles," J. Sound Vib. **304**, 400–406 (2007).
[28]M. Saeki, "Impact damping with granular materials in a horizontally vibrating system," J. Sound Vib. **251**, 153–161 (2002).
[29]Z. Xu, M. Wang, and T. Chen, "An experimental study of particle damping for beams and plates," ASME J. Vibr. Acoust. **126**, 141–148 (2004).
[30]J. Allard, M. Henry, J. Tizianel, L. Kelders, and W. Lauriks, "Sound propagation in air-saturated random packings of beads," J. Acoust. Soc. Am. **104**, 2004–2007 (1998).
[31]J. Chazot and J. Guyader, "Prediction of sound transmission through double panels filled with granular materials," in Proceedings of Internoise, Honolulu, HI (2006), pp. 227–247.
[32]F. Xin, T. Lu, and C. Chen, "Vibroacoustic behavior of clamp mounted double-panel partition with enclosure air cavity," J. Acoust. Soc. Am. **124**, 3604–3612 (2008).
[33]F. Xin and T. Lu, "Analytical and experimental investigation on transmission loss of clamped double panels: Implication of boundary effects," J. Acoust. Soc. Am. **125**, 1506–1517 (2009).
[34]P. Debergue, R. Panneton, and N. Atalla, "Boundary conditions for the weak formulation of the mixed (u,p) poroelasticity problem," J. Acoust. Soc. Am. **106**, 2383–2390 (1999).
[35]R. Daniel, A. Poloski, and A. Sez, "A continuum constitutive model for cohesionless granular flows," Chem. Eng. Sci. **62**, 1343–1350 (2007).
[36]B. Song, J. Bolton, and Y. Kang, "Effect of circumferential edge constraint on the acoustical properties of glass fiber materials," J. Acoust. Soc. Am. **110**, 2902–2916 (2001).
[37]J. Allard, *Propagation of Sound in Porous Media: Modelling Sound Absorbing Materials* (Chapman and Hall, London, 1993).